WATER RESOURCES RESEARCH, VOL. 37, NO. 9, PAGES 2323–2332, SEPTEMBER 2001

Effect of buoyancy ratio on the development of double-diffusive finger convection in a Hele-Shaw cell

Clay A. Cooper
Desert Research Institute, Reno, Nevada, USA

Robert J. Glass
Flow Visualization and Processes Laboratory, Sandia National Laboratories, Albuquerque, New Mexico, USA

Scott W. Tyler
Department of Environmental and Resource Sciences and Department of Geological Sciences
University of Nevada, Reno, Reno, Nevada, USA

Abstract. We consider the evolution of double-diffusive finger convection for a two-solute (salt-sucrose) system in a Hele-Shaw cell. A high-resolution, full-field, light transmission technique was used to study the development of the instability that resulted from layering a lighter sucrose solution over a denser salt solution. The buoyancy ratio (R_ρ), which is a ratio of fluid density contributions by the two solutes and defines the degree of system disequilibrium, was varied systematically from conditions that were nearly stable ($R_\rho = 2.8$) to those that were moderately unstable ($R_\rho = 1.4$). In all experiments, fingers are found to form continuously throughout time from a finger "generation" zone that straddles the location of the initial interface between solutions. At low R_ρ, fingers develop rapidly, merge with adjacent fingers, and grow far beyond the finger generation zone through a series of finger "conduits." In the higher R_ρ experiments, fingers are slower to evolve, do not interact as dynamically, and do not grow far beyond the generation zone. Solute mass fluxes at low R_ρ quickly reach a constant many times greater than that of a purely diffusive system; at high R_ρ, mass fluxes decay as $t^{-1/2}$ and behave diffusively but with effective diffusion coefficients much greater than those for molecular diffusion.

1. Introduction

When multiple density-affecting solutes are dissolved in a buoyantly stable fluid, the different rates of molecular diffusion can result in the development of small-scale structures that lead to an enhanced rate of mass transport. The structures that develop are the result of a hydrodynamic instability; their qualitative and quantitative features are very different from those associated with stable advective, dispersive, and/or diffusive transport. Consider the situation where two solutions are layered, with the less dense solution on top. Two different modes of double-diffusive motion can result depending upon whether the faster or slower diffusing solute is dissolved in the top layer. If the faster diffusing solute is on top, a parcel of fluid perturbed downward across the interface diffuses mass outward more rapidly than it gains mass from the slower diffusing solute. It then becomes less dense than the surrounding fluid, moves upward, and overshoots its original position before repeating the motion. This is the oscillatory mode of double-diffusive convection. Alternatively, if the slower diffusing solute is on top, a parcel of fluid perturbed downward takes on mass from the surrounding faster diffusing solute more rapidly than it diffuses its own slower diffusing solute so that the parcel continues to fall. Likewise, parcels of fluid perturbed upward continue to rise. This mode is termed double-diffusive fingering because it leads to a set of upward and downward growing fingers. In either system it is diffusion of the component stabilizing to the vertical density gradient that destabilizes the system. For example, in the case of the finger instability, diffusion of the faster diffusing solute allows the release of potential energy of the slower diffusing solute, resulting in convection. Hence diffusion is both a driver and a brake in these systems.

The finger instability was hypothesized to occur in parts of the low to middle latitudes of the world's oceans for many years before techniques were developed to detect and confirm its presence in the 1970s. In the ocean, fingers are created as a result of a difference in diffusivities between heat and solute. Water above the thermocline is warmer and saltier than that below, resulting in thermohaline (double-diffusive finger) convection. Thermohaline convection has been shown to be an important control on the balance of heat and salt in the ocean and to drive large-scale circulation where it occurs. Guided by the experience of the oceanographic community of the 1960s, *Green* [1984], *Imhoff and Green* [1988], *Phillips* [1991], and *Cooper et al*. [1997] have hypothesized the existence of subsurface environments (porous media and fractures) favorable to double-diffusive finger convection. These include environments where multiple dissolved density-affecting components are present, i.e., deep circulation in marine and terrestrial alluvial basins; interaction between groundwater and playas, estuaries, and other bodies of surface water; circulation of fluids in metamorphic environments; and transport of dissolved solutes from solid waste landfills.

Paper number 2001WR000343.
0043-1397/01/2001WR000343$09.00

Table 1. Experiments Analyzed[a]

Experiment	R_ρ	$k \times 10^8$ m^2	Δc_2, kg kg^{-1}	Time to Fingers Reaching Boundary, min	Experiment Duration, hours
1[b]	1.4	2.14	0.01381	187	13
2[b]	1.8	2.14	0.01088	658	72
3[c]	2.4	2.21	0.00826	3767	337.8
4[b]	2.8	2.14	0.00710	NA	90.5

[a]Diffusion coefficients are $D_1 = 1.57 \times 10^{-9}$ m^2 s^{-1} (NaCl) [*Stokes*, 1950]; $D_2 = 5.53 \times 10^{-10}$ m^2 s^{-1} (sucrose) [*Gosting and Morris*, 1949]; cell height $h = 31$ cm; concentration difference $\Delta c_1 = 0.01088$ kg kg^{-1}; kinematic viscosity $v = 1.025 \times 10^{-6}$ m^2 s^{-1} [*Weast*, 1977]; $g = 9.81$ (sin 25°) m s^{-2} (the angle of the cell was 25° to horizontal); solute expansion coefficients (β) for NaCl and sucrose are -0.755 and -0.415, respectively [*Weast*, 1977]. The values of the solutal Rayleigh numbers Rs_i reported by *Cooper et al*. [1997] are based upon l, an initial vertical length scale representation of local gradients that is intrinsic to the onset of convection. NA means fingers did not reach the horizontal boundaries in this experiment.
[b]Dye concentration, 0.125 g kg^{-1} in NaCl solution.
[c]Dye concentration, 0.125 g kg^{-1} in sucrose solution.

The behavior of a developing double-diffusive convection system is affected by the magnitude of its deviation from the equilibrium state toward which the system evolves [*Turner*, 1979]. One measure of the degree of disequilibrium in these systems utilizes the nondimensional solutal Rayleigh number of each component, which for porous media is written

$$Rs_i = \frac{\beta_i \Delta c_i g k H}{D_i v}, \tag{1}$$

where β_i [dimensionless] refers to the expansion coefficient for a component; Δc_i [dimensionless] is the change in concentration of a solute (change in temperature for heat) over some characteristic length H [L]; g is the acceleration due to gravity [L t^{-2}]; k is the intrinsic permeability [L^2]; v is the kinematic viscosity of the solution [L^2 t^{-1}]; D_i is the molecular diffusion coefficient of a component [L^2 t^{-1}]; and the subscripts $i = 1$, 2 refer to the faster and slower diffusing components, respectively. For the case where one or both of the Rayleigh numbers greatly exceeds a critical condition, there is nearly universal agreement that the buoyancy ratio,

$$R_\rho = \frac{\beta_1 \Delta c_1}{\beta_2 \Delta c_2}, \tag{2}$$

emerges as the appropriate dimensionless parameter that defines the degree of disequilibrium. Experiments in ordinary fluids [*Turner*, 1967; *Stern and Turner*, 1969; *Lambert and Demenkow*, 1971; *Griffiths and Ruddick*, 1980; *Taylor*, 1991; *Taylor and Veronis*, 1996], porous media [*Imhoff and Green*, 1988], and Hele-Shaw cells [*Cooper et al*., 1997] have shown that as R_ρ decreases from the stability boundary at τ^{-1} (approximately 80 and 3 for heat/salt and salt/sucrose systems, respectively), the system transitions from being diffusion-dominated to convection-dominated with increasing mass fluxes and finger velocities. The molecular diffusivity ratio τ is defined with the smaller diffusivity in the numerator such that $0 < \tau < 1$.

Here we present the results of a set of experiments conducted in a Hele-Shaw cell that consider system evolution after the onset of instability for the NaCl (sodium chloride) and sucrose system. These experiments were originally used by *Cooper et al*. [1997] to explore the theoretical boundary dividing stable double diffusion and unstable double-diffusive convection in a Hele-Shaw cell. While holding the initial Rs_1 constant (i.e., salt concentration), R_ρ was varied in the experiments (by adjusting the concentration of the lower diffusivity sucrose solution) over a range from nearly stable (2.8) to moderately unstable (1.4), yielding system behavior as a function of the initial degree of disequilibrium. Using a quantitative light transmission technique, we tracked the concentration field of a dye added to one of the solutions as a function of time throughout the course of each experiment. This technique is ideal for capturing detailed structure on the submillimeter scale and larger. Such data allow us to describe the dynamics of the evolving unstable flow field as a function of time through characterization of structural measures, such as the height of the finger generation zone and finger width, as well as mass transfer.

2. Experimental Design

Cooper et al. [1997] presented the results of 12 experiments designed to study the location of the stability boundary for a fluid layered with a solution of sucrose over a solution of sodium chloride (NaCl) in a Hele-Shaw cell. The experiments were conducted in a region of Rayleigh parameter space from $Rs_1 \approx 141{,}000$–$145{,}000$ and $Rs_2 \approx 132{,}000$–$288{,}000$ (based upon the height of the cell). Rs_1 was selected so that solute concentrations might be representative of environmental contamination problems, while Rs_2 was varied to yield buoyancy ratios from 1.4 (most unstable) to 2.8 (nearly stable). While *Cooper et al*. [1997] were only concerned with system stability, here we analyze the data set to consider the evolution of the unstable flow field as a function of R_ρ. The results of four of these experiments that span the same range of parameter space as the original 11 unstable experiments are analyzed in detail (Table 1); the remaining seven experiments were used to confirm qualitative trends. One of the original experiments was stable and thus is not considered here.

Low Reynolds number flows in Hele-Shaw cells can mimic two-dimensional flows through porous media [*Bear*, 1988] and are direct models of flow through smooth-walled fractures. The intrinsic permeability of the cell is $b^2/12$, where b is the cell gap. Conditions on velocities and convective length scales that must be met for analogy with porous systems were discussed in relation to the data by *Cooper et al*. [1997]. Though these conditions were all satisfied, Hele-Shaw cells are still not always exact analogs to porous media as they do not completely model processes such as hydrodynamic dispersion that are dependent upon the pore structure. However, they allow one to study many fundamentals of viscous flow phenomena that are difficult to analyze with experimental porous media. In our case, the Hele-Shaw cell allowed us to use a quantitative

light transmission technique to measure the concentration field of a dye dissolved in one of the solutions, resulting in a temporal sequence of high-resolution concentration images of the entire cell. We emphasize that the concentration field measured is that of the dye. However, given that the evolving convective motion results in mass fluxes many times greater than those due to diffusion, it is assumed that the dye maps the solute (NaCl or sucrose) into whose solution it was added.

2.1. Experimental Apparatus

Experiments were conducted in a transparent Hele-Shaw cell (310 mm tall, 170 mm wide) with a gap between 0.495 and 0.515 mm, depending on the experiment. Impermeable boundaries defined the edges of the cell except for two small regions across the top that allowed air to escape as the cell was filled. The cell was filled from the bottom with a NaCl solution, and a thin plastic slider (0.3 mm thick) was inserted across the cell within a horizontal groove (1.0 mm deep $\times$ 0.4 mm wide) that had been milled horizontally across the center of the inside of each plate. The cell was then filled from above with the sucrose solution. The slider was removed to bring the two solutions in contact and begin the experiment. As the slider was removed, a small transition (mixed) zone between the fluids always resulted. Measurements of the height of this zone by *Cooper et al*. [1997] determined that it varied horizontally across the cell and from experiment to experiment, ranging from 1.1 to 16.4 mm for all experiments (see their Plate 1 for an example image of the initial transition zone).

A light-absorbing dye was added to one of the two solutions so that a quantitative light transmission technique using a full-field diffused light source and electronically cooled and shuttered charge-coupled device (CCD) camera (2048 $\times$ 2048 pixels, 4096 gray levels) could be applied to measure the two-dimensional concentration field in time. Each pixel measured a 0.18 $\times$ 0.18 mm region of the cell (this was incorrectly reported by *Cooper et al*. [1997] as 5.5 pixel mm^{-2}). The concentration of the dye used (0.0005 kg FD&C blue #1 kg^{-1} water or less) increased the solution density by less than 0.2%; its molecular diffusion coefficient has been measured as 5.67×10^{-10} m^2 s^{-1} [*Detwiler et al*., 2000].

2.2. Digital Image Reduction to Quantitative Concentration Fields

Evaluation of our digital image reduction procedure reported by *Cooper et al*. [1997] led to several improvements. All images were first adjusted to remove small temporal fluctuations in light source using a constant-density stepped wedge present in each image. Because the cell was moved between experiments and between each calibration curve image, we then aligned the images by shifting each image using a reference point. Each adjusted and aligned image was then converted to normalized light intensity (I_n) to remove large spatial variations in light transmittance through the cell using the following:

$$I_n = \frac{I_i - I_{\mathrm{cl}}}{I_{\mathrm{dye}} - I_{\mathrm{cl}}}. \tag{3}$$

Here I_i is the gray level of an individual pixel in the image being normalized, and I_{dye} and I_{cl} are reference images for the fully dyed ($c = c_0$) and clear ($c = 0$) conditions. Each pixel was then converted to normalized concentration through a calibration curve relating normalized concentration of the dye (c/c_0) to I_n. The calibration curve was built by measuring the intensity fields within the cell for a series of dye concentrations. Because of slight differences (<5%) in the average gap in the top and bottom of the cell, a separate calibration curve was built for the top and bottom halves. The correlation coefficient was greater than 0.99 for both calibration curves. Accuracy of our method was also checked by tracking the total mass in the cell for every experiment as calculated by taking the concentration image times the Hele-Shaw cell gap field measured using the method of *Detwiler et al*. [1999] and then summing over all points in the image. Mass was found to be conserved to within 1.5% for all images in all experiments, a slight improvement on the image reduction method discussed by *Cooper et al*. [1997], where it was reported as 2%. Evaluation of the precision error at a point using approaches similar to *Detwiler et al*. [1999] and *Detwiler et al*. [2000] showed the combined root-mean-square (RMS) error due to temporal fluctuation (single images with no temporal averaging) and alignment shifts (always greater than one pixel) to be ~4%. Averaging over many points in an image to build concentration profiles or fluxes into regions of the cell yields measures that rapidly decrease the precision based error.

3. Results and Discussion

Each experiment began by removing the slider separating the two solutions in the upper and lower halves of the Hele-Shaw cell. Depending upon the degree of instability, initial perturbations develop either rapidly (low initial R_ρ) or slowly (of the order of several hours for high initial R_ρ), select their own internal length scale, and grow. Plate 1 presents a time series of normalized concentration images for $R_\rho = 1.4$ and 2.8. The images were chosen such that the mean c/c_0 in the upper half of the cell is equivalent for respective images in time and chosen to be 0.029, 0.058, and 0.087. The corresponding times for these images are 52, 166, and 274 min ($R_\rho = 1.4$) and 522, 2993, and 6871 min ($R_\rho = 2.8$). Late-time images are shown in Plate 2 for $R_\rho = 1.4$, 1.8, and 2.4 corresponding to times of 678, 3378, and 15,282 min, respectively, and a common mean c/c_0 in the upper half of the cell of 0.20. A late-time image for $R_\rho = 2.8$ is not shown because the experiment was terminated before this concentration was reached. Across Plates 1 and 2 we clearly see R_ρ to influence concentration field structure, finger velocity, and timescale. In the following, we describe the temporal evolution of the concentration fields (section 3.1); structural measures, including concentration profiles, finger generation zone height, and finger width (section 3.2); and the transfer of mass as a function of R_ρ (section 3.3).

3.1. General Description of Evolving Concentration Fields

Animations of the concentration fields taken over the course of each experiment show a rich and complex behavior. For $R_\rho = 1.4$, fingers develop from a region straddling the initial transition zone and lengthen. As fingers lengthen, they may either pinch off at their root within the original transition zone, or they may continue to grow. New fingers are continuously generated from the center of the cell in a region we call the finger "generation" zone. This zone slowly grows vertically in time, and for $R_\rho = 1.4$ fingers always extend well beyond. Often, new fingers ("followers") that develop within the generation zone become entrained within established older fingers ("leaders"). The follower fingers travel slightly faster and eventually overtake the leader fingertip. In addition, outside the

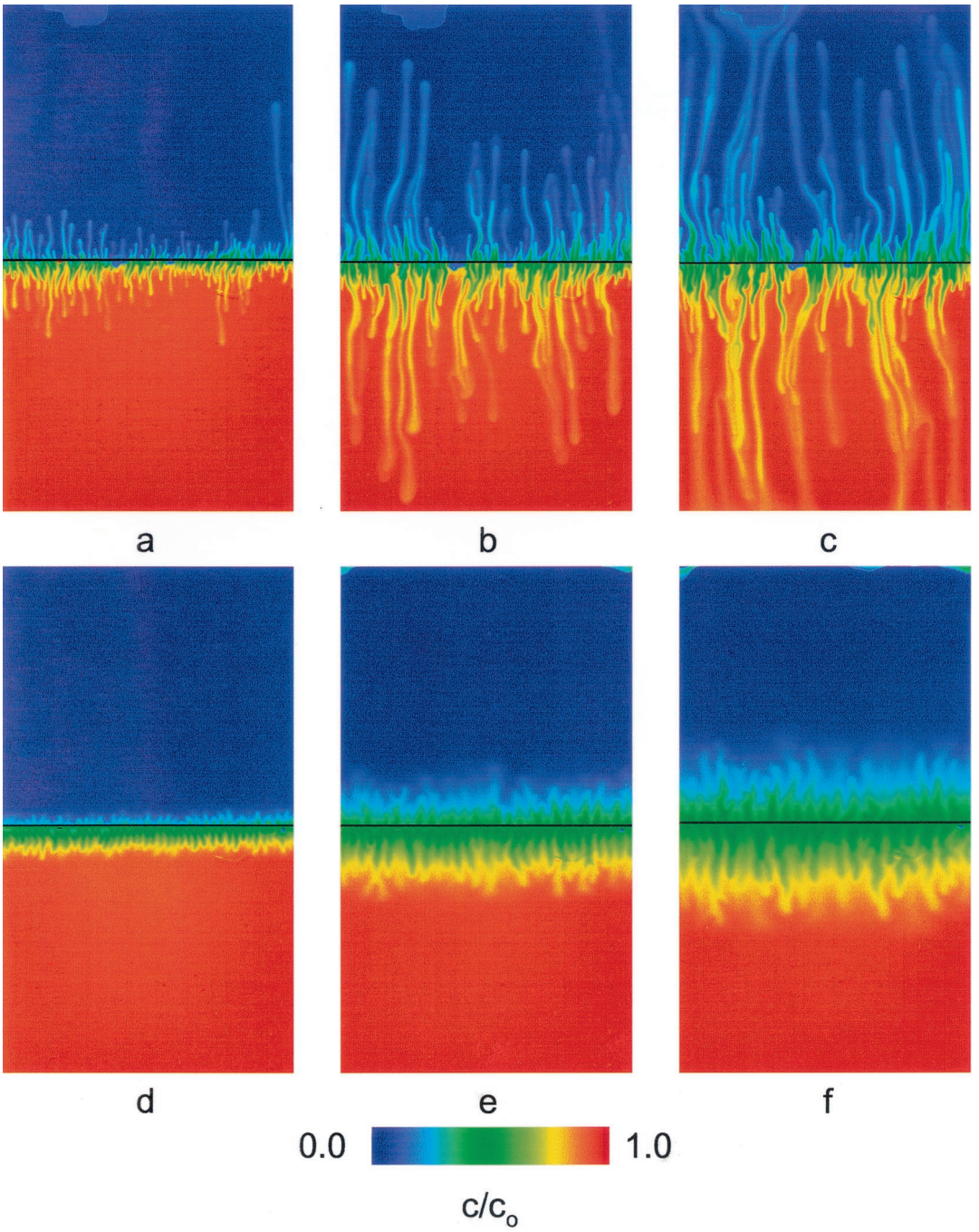

Plate 1. Evolution of the c/c_0 field for experiment with (top row) $R_\rho = 1.4$ and (bottom row) $R_\rho = 2.8$. Images were chosen for mean half-cell c/c_0 for the $R_\rho = 1.4$ experiment as (a) 0.029 at 52 min, (b) 0.058 at 166 min, and (c) 0.087 at 274 min; for the $R_\rho = 2.8$ experiment they are (d) 0.029 at 522 min, (e) 0.058 at 2993 min, and (f) 0.087 at 6871 min. The black line across the center of the cell shows the location of the slot where the plastic slider was removed to begin the experiment. Field dimensions are 16.2 cm wide by 28.3 cm tall.

generation zone, adjacent fingers often merge, resulting in a preferred spacing between fingers greater than their spacing within the generation zone. Repetition of entrainment and merger results in a series of "conduits" along which upward and downward moving fingers travel. Within a conduit a stair step concentration field is evident as several fingers follow the leader (Figure 1). With time, as the generation zone height increases, wider fingers develop within. As a result, longer, wider fingers can form before adjacent fingers become entrained and merge into finger conduits.

The evolving pattern of continuously developing and coalescing (merging) fingers progresses throughout the experiment as long as the criterion for instability is met. There is a very strong symmetry between the patterns that form in the upper and lower halves of the cell. As fingers reach the upper and lower cell boundaries, they create layers of lower- and

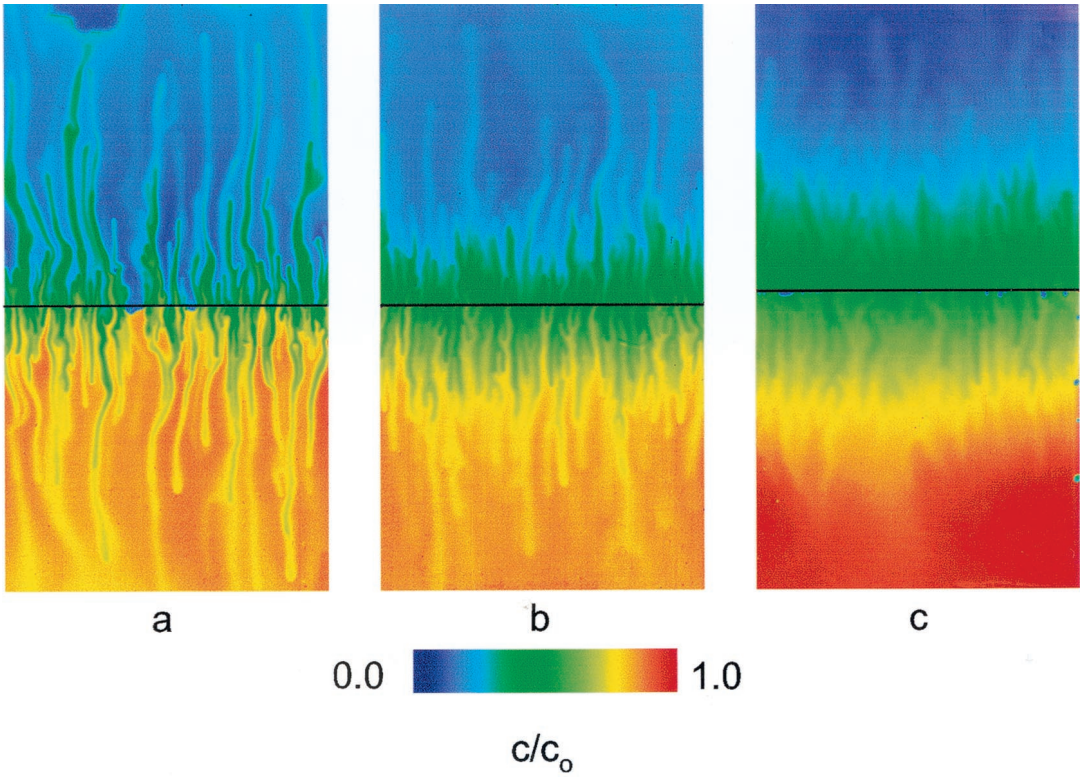

Plate 2. Comparison of late-time c/c_0 fields at a mean half-cell $c/c_0 = 0.20$ for (a) $R_\rho = 1.4$ at 678 min, (b) $R_\rho = 1.8$ at 3378 min, and (c) $R_\rho = 2.4$ at 15,282 min. Since the dye was dissolved in the sucrose for the $R_\rho = 2.4$ experiment and was dissolved in the sodium chloride for the other two experiments, we show for comparison $1 - c/c_0$ for $R_\rho = 2.4$ in Plate 2c. Field dimensions are 16.2 cm wide by 28.3 cm tall.

higher-density fluid, respectively, there. The result is a greater density difference than at the start of the experiment; in time these layers at the upper and lower cell boundaries thicken vertically, mix with fluid between conduits, convect toward the center of the cell and eventually feed the growing generation zone. Thus, although the global fluid density gradient becomes steeper in time, the individual concentration gradients that drive the system within the finger generation zone decrease, causing the eventual rundown of convection.

With increasing R_ρ, the development and structure of the unstable flow field slowly transitions as the diffusive and convective timescales converge. Fingers travel slower and somewhat straighter and have larger diffuse regions around them than at lower R_ρ. Pinching off within the transition zone becomes less frequent, and fingers do not extend as far beyond the generation zone as compared with the low R_ρ experiments. At $R_\rho = 2.8$, initial fingers travel only ~1–2 cm before completely stalling and diffusing into the background. In this highest R_ρ experiment, new fingers that subsequently form still seem to follow the path of old fingers (as at lower R_ρ) and grow outward a bit farther each time before stalling and diffusing. Thus, as R_ρ increases, the solute mass remains closer to the original transition zone, and as comparison of late-time images in Plate 2 shows, fingers become wider and more diffuse.

3.2. Structural Measures

Concentration fields can be integrated horizontally to yield average concentration profiles. Figure 2 shows the profiles for the concentration fields shown in Plate 1. All the profiles are nearly symmetric about the center of the cell. For $R_\rho = 1.4$ (Figure 2a) a clear characterization of the generation zone is seen as the near-linear region between approximately 0.16 and 0.84 (i.e., ±1 standard deviation centered about c/c_0 of 0.5). Outside of this zone the sharp change in slope depicts solute mass that is being transported out of the generation zone by fingers into the tails of the profile. For $R_\rho = 2.8$ (Figure 2b) the profiles appear much more diffusive and lack the convective behavior in the tails, as fingers do not grow far outside of the generation zone. A diffusion solution with an "enhanced" diffusion coefficient of 4×10^{-9} m^2 s^{-1} is plotted for comparison. The choice of D is discussed in section 3.3.

Profiles for the late-time fields (Figure 2c) show a much greater concentration spread about the center of the cell. For $R_\rho = 1.4$ the near-linear profile through the center of the cell is confined to the distance encompassed by c/c_0 between approximately 0.3 and 0.7. The concentrations at the top and bottom of the cell for $R_\rho = 2.4$ are still nearly 0 and 1, as few fingers have reached the cell boundaries. For $R_\rho = 1.8$ and 1.4, many fingers have reached the boundaries, and at $R_\rho = 1.4$ the concentration profile has begun to invert to form stable layers of more dense (bottom) and less dense (top) fluid. As mentioned above, this fluid mixes and is carried back toward the center of the cell between the convective conduits to eventually feed the generation zone.

Figure 3 shows the growth in time of the generation zone (h) for the four experiments. We define h operationally as the distance covered by 1 standard deviation of the c/c_0 field above and below the horizontal centerline of the cell (i.e., concentrations of 0.16 and 0.84, respectively). The generation zone

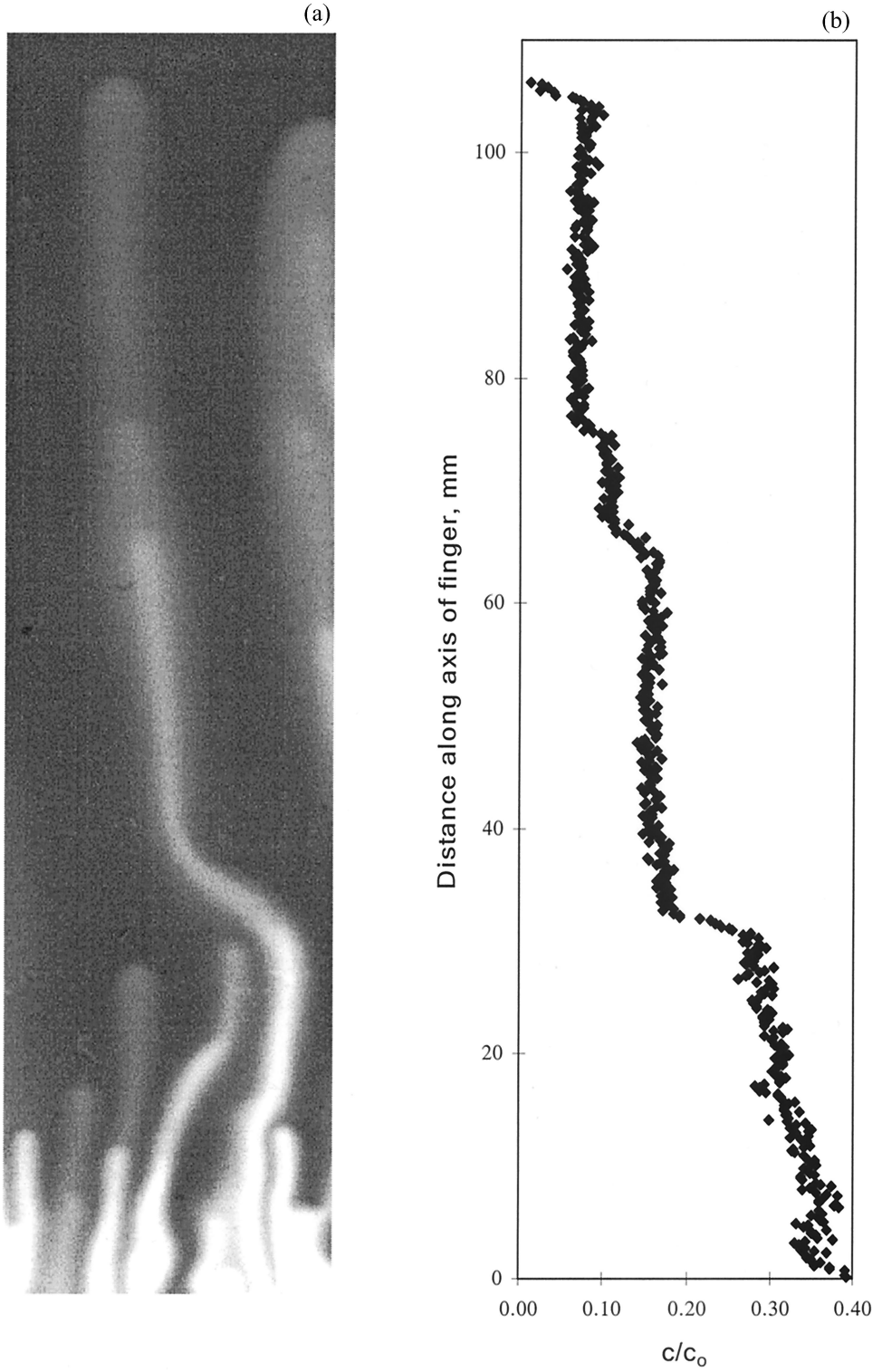

Figure 1. Normalized concentration profile along a conduit with several follower fingers. The conduit (Figure 1a) shows the stair-step pattern represented by the leader finger with individual followers; the corresponding concentration profile (single pixel wide) along the axis of the finger is shown in Figure 1b. Scatter in the concentration profile is representative of the ~4% RMS point wise error.

grows nearly linear in time in the most unstable experiment, but as only $t^{1/2}$ in the more stable experiments, i.e., initial R_ρ of 2.4 and 2.8. These results are consistent with those of *Taylor and Veronis* [1996] who showed linear behavior with $R_\rho < 2.5$ and $t^{1/2}$ behavior for larger values of R_ρ in laboratory tank experiments (i.e., nonporous systems). The break in slope at 800 min for $R_\rho = 1.4$ is an artifact of our operable definition of the linear generation zone. Beyond this time the concentrations defining the generation zone have shortened from 1 standard deviation in c/c_0 (e.g., see the profile for $R_\rho = 1.4$ in Figure 2c).

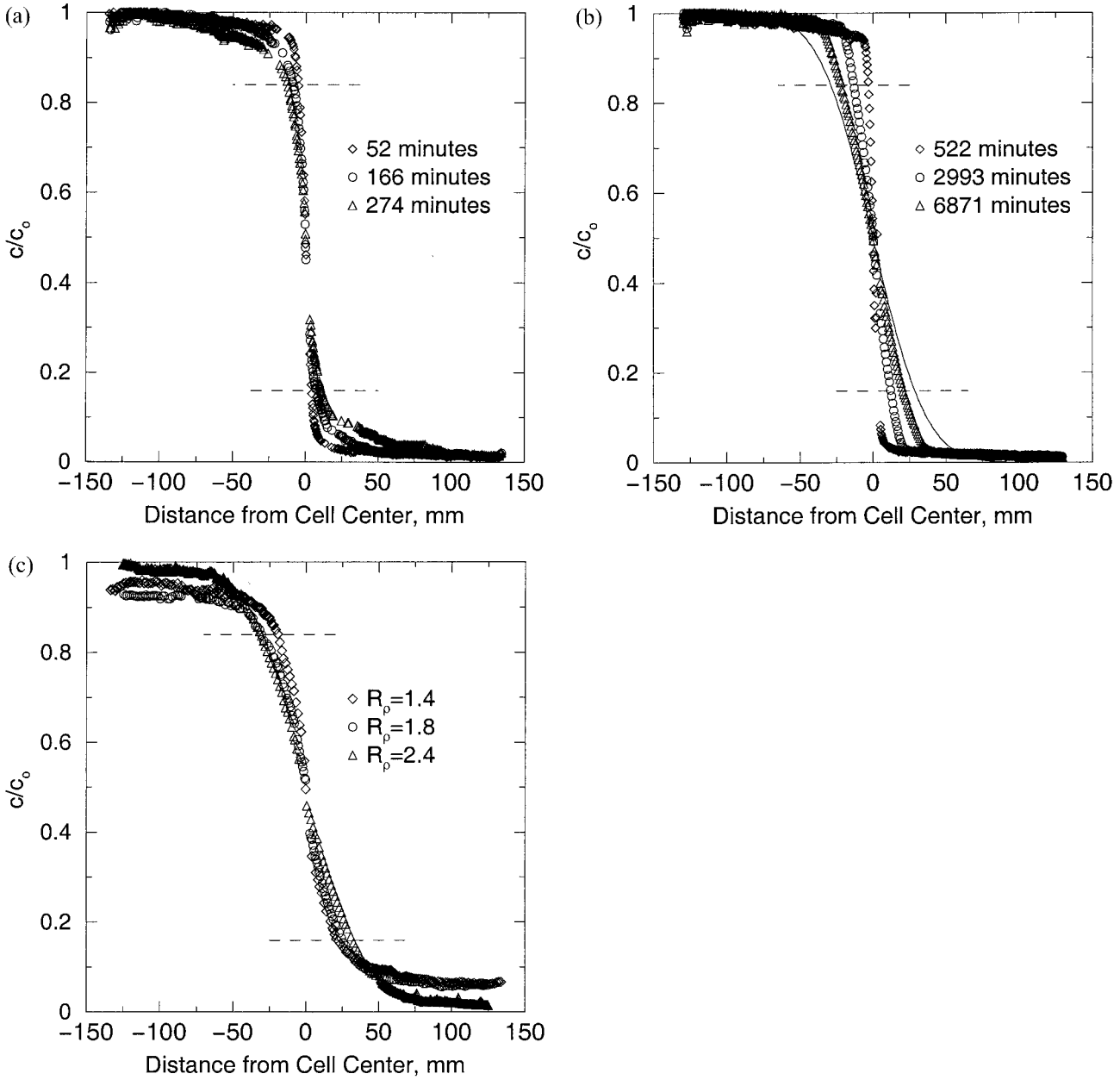

Figure 2. Horizontally averaged c/c_0 (across the cell) when the mean c/c_0 in the upper half of the cell is 0.029, 0.058, and 0.087 for the (a) $R_\rho = 1.4$ and (b) $R_\rho = 2.8$ experiments. Shown in Figure 2c are horizontally averaged c/c_0 across the cell for the $R_\rho = 1.4$, 1.8, and 2.4 experiments when the mean c/c_0 in the upper half of the cell is 0.2. The horizontal dashed lines are located at ± 1 standard deviation of the concentration field (i.e., $c/c_0 = 0.16$ and 0.84, respectively). Shown in Figure 2b is an error function solution to transient diffusion in an infinite half-space with $D = 4 \times 10^{-9}$ m^2 s^{-1} and $t = 250$ min. The data support a model for transport in high R_ρ systems that are diffusive-like.

Finger width at the location of the original transition zone is plotted as a function of time in Figure 4. Finger width (w) was measured by counting the number of fingers across a portion of the cell and dividing by this distance. In general, fingers widen in time as $\sim t^{1/2}$. This result is consistent with theoretical results where the width of equilibrium fingers and those with maximum growth rates should be proportional to the buoyancy layer scale, which is defined as the horizontal distance where concentration differences are adjusted across finger boundaries [*Veronis*, 1987].

3.3. Mass Transfer

Figure 5 shows the temporal change in mean c/c_0 in half of the cell for each experiment. Also shown are the times in which the first fingers reached the top and bottom of the cell. For $R_\rho = 1.4$ the relationship is linear and remains so long after the first fingers have reached the upper and lower cell boundaries. The $R_\rho = 1.8$ experiment shows linear behavior before and for some time after (~600 min) the fingers reach the top and bottom of the cell. Beyond this time the increase of mean

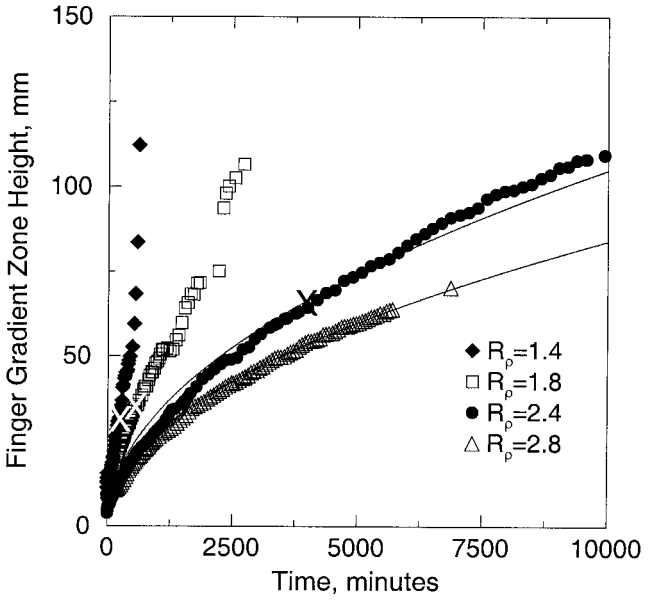

Figure 3. Growth of the finger generation zone (h) defined by the distance encompassed by ± 1 standard deviation of the horizontally averaged c/c_0 field. Also shown are $t^{1/2}$ curves to show that transport agrees with diffusive behavior for the R_ρ = 2.8 experiment but is slightly faster for the R_ρ = 2.4 experiment. For the R_ρ = 1.4 and 1.8 experiments, measurement of the zone became vague, as upward traveling fingers met the oppositely moving advective mass to create a large vertical zone of nearly constant concentration. Therefore not all of the late-time data are plotted.

concentration in the upper half of the cell slows. For the two experiments nearest stability (initial R_ρ = 2.4 and 2.8), the time rate of change in concentration is very nearly $t^{1/2}$.

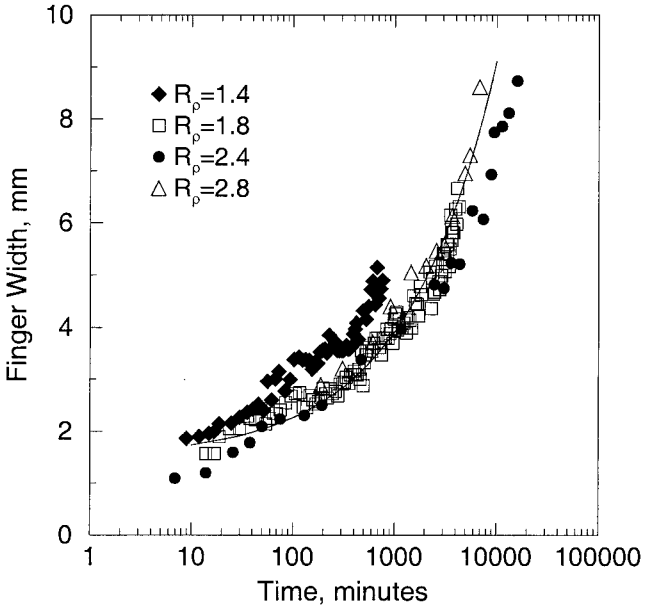

Figure 4. Growth of finger widths showing that merging, branching, and dissipation act collectively to produce a coherent scale change. The most stable experiments have the widest fingers. The solid $t^{1/2}$ curve shows that, in general, fingers widen as $t^{1/2}$.

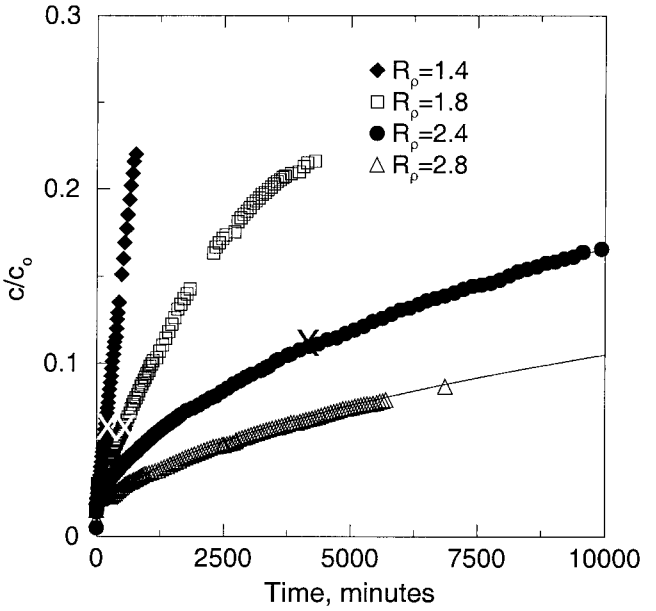

Figure 5. Evolution in time of the mean c/c_0 in half of the Hele-Shaw cell. The cross marks the time at which the fingers reached the cell boundary in each experiment. Fingers did not reach either horizontal boundary in the R_ρ = 2.8 experiment. Also plotted are square root of time curves, showing that R_ρ = 2.4 and 2.8 approximate diffusive behavior; the curve for R_ρ = 2.4 exactly overlies the data.

Figure 6 shows the temporal behavior of the normalized mass flux across the centerline of the initial profile for each experiment. We note that this result for the dye should represent the density-affecting component reasonably well for all

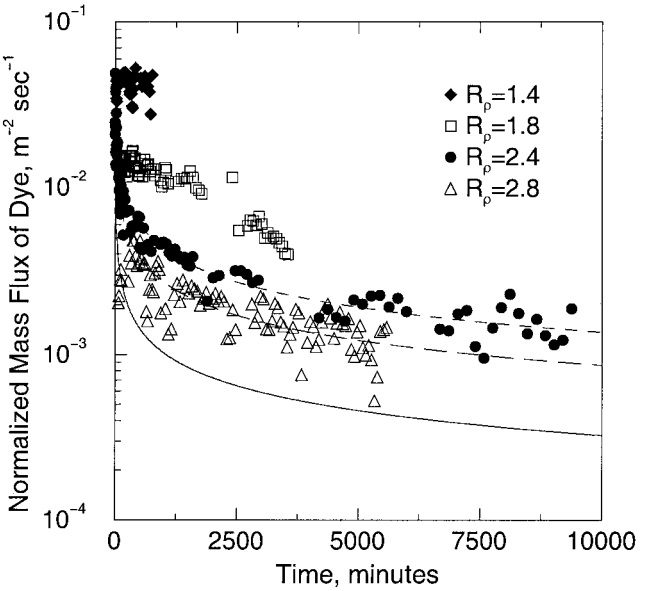

Figure 6. Temporal behavior of mass fluxes normalized by the total dye mass for all four experiments. Second-order finite differences in time were used for calculations. Solid lines are one-dimensional solutions to the diffusion equation for similar initial and boundary conditions. Although fingering is advective, for the two highest R_ρ experiments, the data fit a diffusive model reasonably well with effective diffusion coefficients of 10^{-8} m^2 s^{-1} for R_ρ = 2.4 and 4×10^{-9} m^2 s^{-1} for R_ρ = 2.8.

experiments, as each is convectively dominated. The $R_\rho = 1.4$ experiment shows constant flux in time, while at $R_\rho = 1.8$, constant flux is found prior to the fingers reaching the horizontal boundaries followed by a decay. Also plotted in Figure 6 is the one-dimensional solution for diffusive flux of dye for a step concentration initial condition. Over the period of the test, fluxes for the most unstable experiment ($R_\rho = 1.4$) are approximately 1.5 orders of magnitude greater than those predicted for simple dye diffusion. For the two most stable experiments ($R_\rho = 2.4$ and 2.8), while fluxes are also much greater than predicted, we find the time evolution of mass flux to be diffusion-like with near square root of time behavior. *Taylor and Veronis* [1996] found similar results for experiments in ordinary fluids when $R_\rho > 2.5$. Our direct observations of convective behavior show that for both these experiments, fingers formed that had most of the characteristics of fingers in more unstable experiments. This is an interesting result, as even though the system was unstable and the patterns associated with transport were convective, temporal mass flux behaves in accordance with a diffusive model. Plotted in Figure 6 are diffusion solutions with effective diffusion coefficients that best fit the data of the $R_\rho = 2.4$ and 2.8 experiments (10^{-8} m^2 s^{-1} and 4×10^{-9} m^2 s^{-1}, respectively). These effective diffusion coefficients are significantly enhanced by nearly 1–2 orders of magnitude beyond the molecular diffusion coefficient of the dye (5.67×10^{-10} m^2 s^{-1}).

4. Concluding Remarks

Our experiments elucidate the dynamics of double-diffusive finger convection as a function of the degree of initial system disequilibrium. For all experiments we discover that fingers form continuously within a finger "generation" zone that straddles the location of the original solution interface. For low R_ρ, fingers rapidly develop, merge with adjacent fingers, and grow outside of the generation zone to the top and bottom boundaries. Newly generated fingers tend to follow the paths of earlier fingers outside the generation zone to form conduits along which fingers course. The height of the finger generation zone grows linearly in time, and solute flux quickly reaches a constant value many times greater than that expected to occur in similar, though stable, diffusive systems. At higher R_ρ, fingers are slower to evolve and do not interact as dynamically as in the lower R_ρ systems. The temporal solute flux for high R_ρ decays as $t^{-1/2}$ and can be mimicked with a diffusive model using an effective diffusion coefficient. This diffusive-like behavior is significant, as the structure within the finger generation zone is still convective in nature.

Finally, we note that large-scale circulation was not observed within the top and bottom solutions in any of our experiments. This result is supported by those of others for both Hele-Shaw cells [*Taylor and Veronis*, 1986; *Shen and Veronis*, 1991; *Stockman et al*., 1998] and porous media [*Imhoff and Green*, 1988]. These observations are important because such circulation occurs in ordinary fluids, i.e., nonporous media, and acts to limit the vertical growth of fingers. Thus, in porous media where viscous forces are large relative to inertial forces, limits on finger growth are yet to be understood; the various "secondary" instabilities analyzed by *Stern* [1969, 1975], *Holyer* [1984], and *Howard and Veronis* [1987, 1992], which act to limit finger growth in ordinary fluids, cannot exist in low Reynolds number systems. An intriguing possibility suggested by our observations is that the merging and subsequent formation of conduits along which fingers travel could be repeated at larger and larger scales. Thus, instead of finger growth being limited, larger and greater-spaced conduits for mass transport may naturally evolve in porous media, leading to growth bounded on a much larger scale than has been observed in any laboratory experiments.

Acknowledgments. Financial support for this research was provided by the U.S. Department of Energy's Basic Energy Sciences Geoscience Research Program under contracts DE-FG03-96ER14611 (Desert Research Institute) and DE-AC04-94AL85000 (Sandia National Laboratories). Experiments were conducted in the Flow Visualization and Processes Laboratory at Sandia National Laboratories. We thank Russ Detwiler for discussions on error within transmitted light systems and Scott Pringle for constructive comments on the manuscript. We also gratefully acknowledge the constructive reviews by Paul Imhoff, Craig Simmons, and an anonymous reviewer.

References

Bear, J., *Dynamics of Fluids in Porous Media*, 764 pp., Dover, Mineola, N.Y., 1988.

Cooper, C. A., R. J. Glass, and S. W. Tyler, Experimental investigation of the stability boundary for double-diffusive finger convection in a Hele-Shaw cell, *Water Resour. Res*., *33*, 517–526, 1997.

Detwiler, R. L., S. E. Pringle, and R. J. Glass, Measurement of fracture aperture fields using transmitted light: An evaluation of measurement errors and their influence on simulations of flow and transport through a single fracture, *Water Resour. Res*., *35*, 2605–2617, 1999.

Detwiler, R. L., H. Rajaram, and R. J. Glass, Solute transport in variable-aperture fractures: An investigation of the relative importance of Taylor dispersion and macrodispersion, *Water Resour. Res*., *36*, 1611–1625, 2000.

Gosting, L. J., and M. S. Morris, Diffusion studies on dilute aqueous sucrose solutions at 1° and 25° with the Gouy interference method, *J. Am. Chem. Soc*., *71*, 1998–2006, 1949.

Green, T., Scales for double-diffusive fingering in porous media, *Water Resour. Res*., *20*, 1225–1229, 1984.

Griffiths, R. W., and B. R. Ruddick, Accurate fluxes across a salt-sugar finger interface deduced from direct density measurements, *J. Fluid Mech*., *99*, 85–95, 1980.

Holyer, J. Y., The stability of long, steady, two-dimensional salt fingers, *J. Fluid Mech*., *147*, 169–185, 1984.

Howard, L. N., and G. Veronis, The salt finger zone, *J. Fluid Mech*., *183*, 1–23, 1987.

Howard, L. N., and G. Veronis, Stability of salt fingers with negligible diffusivity, *J. Fluid Mech*., *239*, 511–522, 1992.

Imhoff, P. T., and T. Green, Experimental investigation of double-diffusive groundwater fingers, *J. Fluid Mech*., *188*, 363–382, 1988.

Lambert, R. B., and J. W. Demenkow, On the vertical transport due to fingers in double diffusive convection, *J. Fluid Mech*., *54*, 627–640, 1971.

Phillips, O. M., *Flow and Reactions in Permeable Rocks*, 285 pp., Cambridge Univ. Press, New York, 1991.

Shen, C. Y., and G. Veronis, Scale transition of double-diffusive finger cells, *Phys. Fluids*, *3*, 58–68, 1991.

Stern, M. E., Collective instability of salt fingers, *J. Fluid Mech*., *35*, 209–218, 1969.

Stern, M. E., *Ocean Circulation Physics*, Academic, San Diego, Calif., 1975.

Stern, M. E., and J. S. Turner, Salt fingers and convecting layers, *Deep Sea Res*., *16*, 497–511, 1969.

Stockman, H., R. J. Glass, C. A. Cooper, and H. Rajaram, Accuracy and computational efficiency in 3D dispersion via lattice-Boltzmann: Models for dispersion in rough fractures and double-diffusive fingering, *Int. J. Mod. Phys. C*, *9*, 1545–1557, 1998.

Stokes, R. H., The diffusion coefficients of eight univalent electrolytes in aqueous solution at 25°, *J. Am. Chem. Soc*., *72*, 2243–2247, 1950.

Taylor, J., Laboratory experiments on the formation of salt fingers after the decay of turbulence, *J. Geophys. Res*., *96*, 12,497–12,510, 1991.

Taylor, J., and G. Veronis, Experiments on salt fingers in a Hele Shaw cell, *Science*, *231*, 39–41, 1986.

Taylor, J., and G. Veronis, Experiments on double-diffusive sugar-salt fingers at high stability ratio, *J. Fluid Mech*., *321*, 315–333, 1996.

Turner, J. S., Salt fingers across a density interface, *Deep Sea Res*., *14*, 599–611, 1967.

Turner, J. S., *Buoyancy Effects in Fluids*, 368 pp., Cambridge Univ. Press, New York, 1979.

Veronis, G., The role of the buoyancy layer in determining the structure of salt fingers, *J. Fluid Mech*., *180*, 327–342, 1987.

Weast, R. C. (Ed.), *CRC Handbook of Chemistry and Physics*, 57th ed., CRC Press, Boca Raton, Fla., 1977.

C. A. Cooper, Desert Research Institute, 2215 Raggio Parkway, Reno, NV 89512-1095, USA. (clay@dri.edu)

R. J. Glass, Flow Visualization and Processes Laboratory, Sandia National Laboratories, P.O. Box 5800, Albuquerque, NM 87185-0735, USA.

S. W. Tyler, Department of Geological Sciences, University of Nevada, Reno, Reno, NV 89557-0180, USA. (styler@unr.edu)

(Received July 14, 2000; revised March 28, 2001;
accepted April 24, 2001.)